# Unsteady Aerodynamics of Nonplanar Wings and Wing-Tail Configurations of Elastic Flight Vehicles in Supersonic Flight

Jack Morito Ii* and William S. Rowe†
*The Boeing Company, Seattle, Wash.*

**This paper presents a method for predicting the unsteady aerodynamic loadings of flexible aircraft with nonplanar wings and wing-tail surfaces in supersonic flow. The aerodynamic interference between the wing and tail has been taken into account. The computation considers dihedral angles on both wing and tail, and longitudinal and vertical separations between them. The aerodynamic influence coefficients (AIC) associated with velocity potential, upwash, sidewash, and longitudinal wash at the center of the arbitrarily oriented pulse-receiving panel are developed. The AIC's are manipulated to avoid numerical integration problems due to their singular natures at the Mach hyperbola. The boundary conditions of the "interfered" surfaces in the disturbed flowfield are discussed. Illustrative examples for the computed aerodynamic quantities and flutter stability boundaries are presented and correlated with empirical data.**

## Nomenclature

$a$ = speed of sound = $U/M$
$A(n,m)$ = integration area of box $n,m$
$b_1$ = chordwise dimension of Mach box
$C_{\bar{\nu}\bar{\mu}\bar{\lambda}}$ = spatial AIC for velocity potential
$\binom{xy}{ab}$ = spatial AIC giving velocity potential at a point on surface "$xy$" because of constant outward normal wash over a box on surface "$ab$"
$C_{\bar{\nu}\bar{\mu}\bar{\lambda}}$
$C_{\bar{\nu}\bar{\mu}\bar{0}}, C_{\bar{\nu}\bar{\mu}}$ = planar AIC for velocity potential
$\Delta C_{pj}{}^{n,m}$ = pressure coefficient difference at box $n,m$ for the $j$th mode
$c$ = local reference chord
$f_j(x,y)$ = $j$th mode shape deflection at $(x,y)$
$\bar{f}_j{}^{n,m}$ = scaled modal displacement at box $n,m$
$k_s, k_l$ = reduced frequencies; $k_s = s\omega/U$ and $k_1 = b_1\omega/U$
$\bar{k}_1$ = nondimensional number = $k_1M^2/\beta^2$
$L_j{}^{n,m}$ = lift on box $n,m$ for the $j$th mode
$M$ = Mach number
$N_{xyz}{}^{n,m}$ = normal wash at box $n,m$ on surface "$xyz$" due to local source strength, where possible subscript values are:
$x = \begin{cases} R\text{-right} \\ L\text{-left} \end{cases}$ $y = \begin{cases} U\text{-upper} \\ L\text{-lower} \end{cases}$ $z = \begin{cases} W\text{-wing} \\ T\text{-tail} \end{cases}$
$\hat{N}_{\substack{xyz \\ abc}}{}^{n,m}$ = normal wash at box $n,m$ on surface "$xyz$" resulting from source strengths on surface "$abc$"
$n_c, m_c, l_c$ = sending surface coordinate system
$\bar{n}_c, \bar{m}_c, \bar{l}_c$ = receiving point coordinate system
$\Delta p(x,y,t)$ = pressure difference between upper and lower surface at $(x,y)$ and at time $t$
$Q_{ij}$ = generalized force due to the deformation in the $i$th elastic mode and loading for the $j$th modal deflections
$q$ = dynamic pressure freestream
$q_j(t)$ = generalized coordinate relating physical deflection to $j$th modal deflections $z(x,y,t) = \Sigma f_j(x,y)\, q_j(t)$
$s$ = wing semispan
$t$ = time
$U$ = freestream velocity
$U_{\bar{\nu}\bar{\mu}\bar{\lambda}}$
$V_{\bar{\nu}\bar{\mu}\bar{\lambda}}$
$W_{\bar{\nu}\bar{\mu}\bar{\lambda}}$ = spatial AIC's for perturbated washes, in the streamwise direction (longitudinal wash), in the spanwise direction (sidewash), in the normal direction (upwash) to the sending surface measured at the receiving point, respectively
$u,v,w$ = perturbation velocities
$x,y,z$ = coordinate system in general
$X,Y,Z$ = global coordinate system
$X_W, Y_W, Z_W$ = wing local coordinate system
$\alpha^{n,m}$ = edge box area ratio for box $n,m$
$\beta$ = $(M^2-1)^{1/2}$
$\bar{\nu},\bar{\mu},\bar{\lambda}$ = $\bar{n}_c, \bar{m}_c, \bar{l}_c$ coordinate location of a pulse sending box
$\xi,\bar{\eta},\bar{\zeta}$ = dummy variables of integration in $\bar{n}_c, \bar{m}_c, \bar{l}_c$ coordinate system
$\phi(x,y,t)$ = perturbated velocity potential at $(x,y)$ and at time $(t)$
$\psi_W, \psi_T$ = dihedral angles of wing and tail, radians positive upward from horizontal
$\omega$ = circular frequency

*Subscripts*

$L$ = lower limit of integration; left-hand surface; lower surface
$R$ = right-hand surface
$T$ = tail
$TE$ = trailing edge
$U$ = upper limit of integration; upper surface
$W$ = wing

*Superscripts*

$(n,m)$
$(\nu,\mu)$ = box location
$(\bar{\ })$ = amplitude

## Introduction

FLUTTER model tests have revealed that aerodynamic interferences can be significant for flutter of variable sweep aircraft.[1,2] Recent studies have shown that the above variations of flutter speed with wing sweep can be predicted for the subsonic case when aerodynamic interference between the wing and horizontal tail is included.[3] However, supersonic trends have not been established analytically, nor have empirical data been obtained to determine more completely the flutter speed trends for higher supersonic Mach numbers. An extensive survey of these interference phenomena on wing-fuselage-tail configurations has been completed by Mykytow et al.[4]

This paper presents a method for predicting the unsteady aerodynamic loadings of flexible aircraft with nonplanar wings and wing-tail surfaces in supersonic flow. The planforms of either surface are entirely general, being specified by linear boundaries between points. The computation considers dihedral angles on both wing and tail and longitudinal and vertical separations between them.

The numerical evaluation of linearized aerodynamic loadings in unsteady supersonic inviscid flow is most effectively achieved in the low-to-moderate supersonic range by using the aerodynamic influence coefficient method of the lifting surface theory (abbreviated AIC), first proposed

Presented as Paper 72-378 at the AIAA/ASME/SAE 13th Structures, Structural Dynamics, and Materials Conference, San Antonio, Texas, April 10–12, 1972; submitted May 5, 1972; revision received September 25, 1972. The work was supported by the Air Force AFFDL Contract F33615-70-C1126. The authors wish to acknowledge the stimulating discussions held with H. Ashley of Stanford University.

Index categories: Nonsteady Aerodynamics; Supersonic and Hypersonic Flow; Aeroelasticity and Hydroelasticity.

* Senior Research Engineer. Member AIAA.
† Research Specialist.

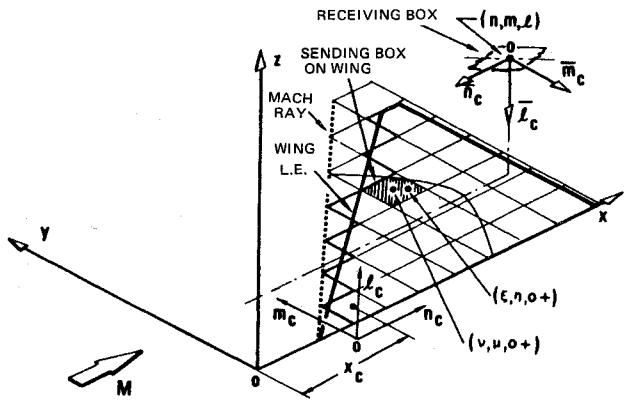


Fig. 1 Receiving point coordinate system.

by Pines, Dugundji, et al.[5,6] The AIC's associated with velocity potential, $C_{\bar{\nu}\bar{\mu}\bar{\lambda}}$, at the center of this receiving box are first computed in the nondimensional coordinate system. The rest of the AIC's for upwash $W_{\bar{\nu}\bar{\mu}\bar{\lambda}}$, sidewash $V_{\bar{\nu}\bar{\mu}\bar{\lambda}}$, and longitudinal wash $U_{\bar{\nu}\bar{\mu}\bar{\lambda}}$, are obtained by differentiating $C_{\bar{\nu}\bar{\mu}\bar{\lambda}}$ by applying the Leibnitz Theorem. These AIC's are manipulated to avoid numerical integration problems due to their singular natures at the Mach hyperbola.

Once the appropriate regions of influence have been determined, and the necessary AIC's calculated, the strength of the unknown source distribution and the local velocity potential difference, $\Delta\phi_j$, are determined by casting these AIC's into matrix form and by taking all possible coupling inside each disturbed region. The boundary conditions to be satisfied are the flow tangency condition on the lifting surface and continuity concepts of mass and pressure on the diaphragm region, respectively.

The pressure distribution for the $j$th mode can be found from the usual linearized expression by differentiating the $\Delta\phi_j$. The lift on a chordwise section and the total lift are computed by integrating the pressure difference. Given the $i$th modal deflection, the associated generalized force due to the $j$th pressure mode, $Q_{ij}$, is computed.

It is well known that the conventional Mach box method may produce inaccurate pressure distributions. Therefore, the refinements, consisting of a subdivision technique,[7] velocity potential smoothing technique,[8] and thickness-correction procedure based on second-order piston theory,[9] are applied. The calculations are made for the AGARD wing-tail configuration for its unsteady aerodynamic applications.

Flutter model test data used in this correlation study are obtained from the experimental flutter results performed for several models tested in the low supersonic Mach number range at Cornell Aeronautical Laboratory.[2]

## Thin Airfoil Theory in Supersonic Flow

Thin airfoil or small perturbation theory is applied to describe the flow patterns that result when small disturbances are superposed on parallel uniform flow. If the time variation of pulsing source singularity is harmonic, the explicit form of the perturbation velocity potential $\phi(x,y,z;t)$ is expressed by an integral equation[10,11]

$$\phi(x,y,z,t) = -\exp(i\omega t)/\pi \int_0^{x-\beta z} d\xi \int_{y-\eta_0}^{y+\eta_0} w_0(\xi,\eta,0+)\exp(-i\omega M(x-\xi)/a\beta^2)\cos(\omega R_h/a\beta^2)/R_h d\eta \qquad (1)$$

for a planform with a supersonic leading edge; 0+ indicates the upper surface of the pulse-sending box; and $R_h = [(x-\xi)^2 - \beta^2\{(y-\eta)^2 + z^2\}]^{1/2}$.

If the planform has a subsonic leading edge, or trailing edge, or a streamwise edge at its tip, "diaphragms" are introduced using the "Evvard concept".[12] The upper and lower surfaces of the planform plus diaphragm can now be considered noncommunicative. Thus the integration area in Eq. (1) is presumed to include any diaphragm regions needed to isolate the upper and lower surfaces, but is restricted to that part of the planform and diaphragm contained inside the forward Mach cone emanating from $(x,y,z)$.

The source distribution that is placed on the diaphragm is initially unknown, and is evaluated using the boundary condition $\Delta p = 0$ at all points not on the wing surface. This condition may be expressed as

$$(\partial/\partial t)\Delta\phi + U\partial/\partial x(\Delta\phi) = 0 \qquad (2)$$

Thus $\Delta\phi = 0$ for an off-wing diaphragm and

$$\Delta\phi(x,y,0,t) = \Delta\phi(x_{TE},y,0)\exp\{ik_1(x-x_{TE})/b_1\}\exp(i\omega t) \qquad (3)$$

for a diaphragm that lies in the wake of the wing.

The wake may have an effect on the wing (if the trailing edge is subsonic) and on the tail. Considerations have so far been based upon purely linearized theory, where the wake coincided with the mean plane of the lifting surface. However, the actual wake deforms in the direction of disturbed free flow and, as is known, tends to roll up. This effect can approximately be taken into account by assuming the actual position of the tail surface relative to the steady wake position to be the effective vertical position at which the unsteady wake will be superimposed.[3]

## Numerical Computation in the Mach Box Grid System

If the integration area may be split into sufficiently small elementary areas, one may make aporoximations in the evaluation of the double integral in Eq. (1). The form of elementary areas presently available for practical computation are squares, the so-called Mach boxes whose diagonals are parallel to the Mach lines, and the so-called characteristic boxes which are rhombuses with sides parallel to the Mach lines. Due to the fact that the Mach box appears to be the most useful and versatile of the elementary shapes proposed to date, the numerical scheme for evaluating the aerodynamic forces used in this study is based on the Mach box method.[6,8,13,14]

In order to establish a convenient counting system for the grid of sending boxes a transformation is made for the wing as

$$n_c = (X_W - X_{CW})/b_1 + 1$$
$$m_c = \beta Y_W/b_1 + 1/2$$

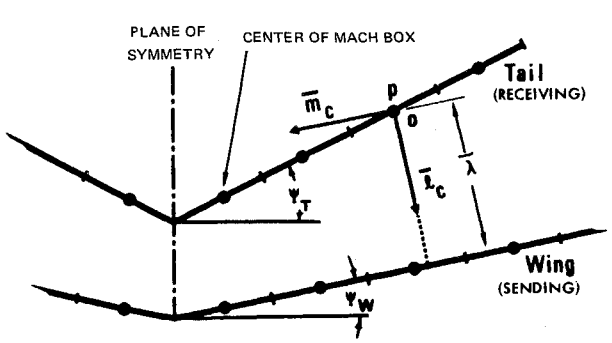


Fig. 2 Receiving point coordinate system in wing-tail configuration.

$$\ell_c = \beta Z_W / b_1$$

where $X_{CW}$ is the location of the first box center on the sending surface and $(X_W, Y_W, Z_W)$ in the wing local coordinate system in which the right wing surface lies on the $X_W Y_W$ plane. A similar transformation is used when the tail is the sending surface.

The location of the receiving point, $(x,y,z)$ in the local coordinate system, is designated $(n,m,l)$ in the $(n_c, m_c, l_c)$ coordinate system, as shown in Fig. 1.

Equation (1) may be expressed in the Mach box grid system

$$\phi_0(x,y,z) = -\frac{1}{\pi} \sum_{\nu}\sum_{\mu} w_{0\nu\mu} \iint_{A(\nu,\mu)} (\exp[-ik_1 M^2(x-\xi)/\beta^2 b_1] \cos[k_1 M R_h/\beta^2 b_1])/R_h \, d\xi \, d\eta \quad (4)$$

$A(\nu,\mu)$ denotes integration over box $(\nu,\mu)$ and $b_1$ is the streamwise dimension of a Mach box.

A final transformation, which is

$$\bar{n}_c = -(n_c - n)$$
$$\bar{m}_c = -(m_c - m)$$
$$\bar{\ell}_c = -(\ell_c - \ell)$$

establishes a nondimensional coordinate system centered on the receiving point (Fig. 1). The location of a sending box is $(\bar{\nu},\bar{\mu},\bar{\lambda})$ in this receiving coordinate system.

The equation for the perturbation velocity potential may now be expressed

$$\phi_0(0,0,0) = \sum_{\nu}\sum_{\mu} w_{0\nu\mu} C_{\nu\mu\bar{\lambda}} \quad (5)$$

where

$$C_{\bar{\xi}\bar{\eta}\bar{\lambda}} = -\frac{1}{\pi} \int_{\bar{\xi}_L}^{\bar{\xi}_U} \int_{\bar{\eta}_L}^{\bar{\eta}_U} \frac{\exp(-ik_1\bar{\xi}) \cos[k_1(\bar{\xi}^2 - \bar{\eta}^2 - \bar{\lambda}^2)^{1/2}/M]}{(\bar{\xi}^2 - \bar{\eta}^2 - \bar{\lambda}^2)^{1/2}} \, d\bar{\xi} \, d\bar{\eta} \quad (6)$$

and is known as an "Aerodynamic Influence Coefficient" or AIC. Also, $\bar{\xi},\bar{\eta}$ are dummy variables of integration and $\bar{\xi}_U, \bar{\xi}_L, \bar{\eta}_U, \bar{\eta}_L$ are the limits of integration associated with the Mach box whose center is at $\bar{\nu},\bar{\mu},\bar{\lambda}$ and are in general functions of $\bar{\nu},\bar{\mu},\bar{\lambda}$. The "pulse-sending" Mach box lies

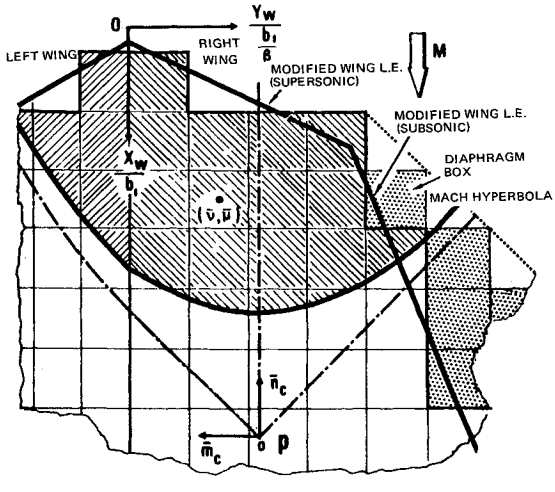


**Fig. 3 Mach box grid systems on sending surfaces and their boundaries.**

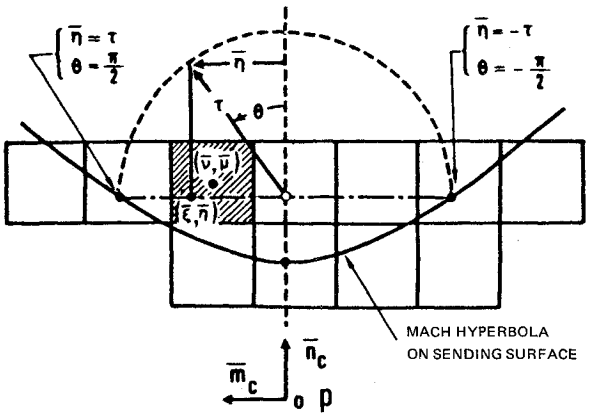


**Fig. 4 Values of $(\tau,\theta)$ corresponding to $(\bar{\xi},\bar{\eta})$.**

wholly or partially inside the forward Mach cone associated with the point (0,0,0).

The upwash at a point $(x,y,z)$ in the local coordinate system can be expressed, by using Eq. (5),

$$w(x,y,z) = \partial\phi/\partial z = \beta/b_1 \, \partial\phi/\partial\bar{\lambda} = \beta/b_1 \sum_{\nu}\sum_{\mu} w_{0\nu\mu} \partial C_{\bar{\nu}\bar{\mu}\bar{\lambda}}(\nu,\mu,\lambda)/\partial\bar{\lambda} \quad (7)$$

The AIC for upwash is therefore defined as

$$W_{\bar{\nu}\bar{\mu}\bar{\lambda}} = \partial C_{\bar{\nu}\bar{\mu}\bar{\lambda}}/\partial\bar{\lambda} \quad (8)$$

Similarly the AIC for sidewash is

$$V_{\bar{\nu}\bar{\mu}\bar{\lambda}} = \partial C_{\bar{\nu}\bar{\mu}\bar{\lambda}}/\partial\bar{\mu} \quad (9)$$

For completeness, the AIC for longitudinal wash is

$$U_{\bar{\nu}\bar{\mu}\bar{\lambda}} = \partial C_{\bar{\nu}\bar{\mu}\bar{\lambda}}/\partial\bar{\nu} \quad (10)$$

Consider, for example, a case of the influence of the right wing on the right tail. The wing and its diaphragm are the sending surface; the receiving points are the centers of the Mach boxes on the tail. Figure 2 shows the general relationship between the surfaces.

If P is the center of a receiving box on the tail, $(\bar{n}_c, \bar{m}_c, \bar{l}_c)$ forms the coordinate system for the analysis where $\bar{n}_c$ disappears into the paper in Fig. 2. Figure 3 shows how the wing looks from $P$.

## Evaluation of Aerodynamic Influence Coefficients

### a) Evaluation of $C_{\bar{\nu}\bar{\mu}\bar{\lambda}}$

The analysis in the previous section has formulated the aerodynamic influence coefficients in the Mach box grid system with reference to the receiving point coordinate system. Since the integrand of $C_{\bar{\nu}\bar{\mu}\bar{\lambda}}$ in Eq. (6) becomes singular at the Mach hyperbola some manipulation of $C_{\bar{\nu}\bar{\mu}\bar{\lambda}}$ is needed to render it amenable to numerical integration. To this end, the function $G(\bar{\xi},\bar{\eta},\bar{\lambda})$ is introduced, where

$$G(\bar{\xi},\bar{\eta},\bar{\lambda}) = \cos[k_1/M(\bar{\xi}^2 - \bar{\eta}^2 - \bar{\lambda}^2)^{1/2}]/(\bar{\xi}^2 - \bar{\eta}^2 - \bar{\lambda}^2)^{1/2} = \partial F(\tau,\bar{\eta})/\partial\bar{\xi} \quad (11)$$

where $F$ is the Bessel function series expressed by

$$F(\tau,\bar{\eta}) = J_0(\bar{k}_1\tau/M)\theta + \sum_{r=1}^{\infty} \frac{(-1)^r}{r} J_{2r}(\bar{k}_1\tau/M) \sin(2r\theta) \quad (12)$$

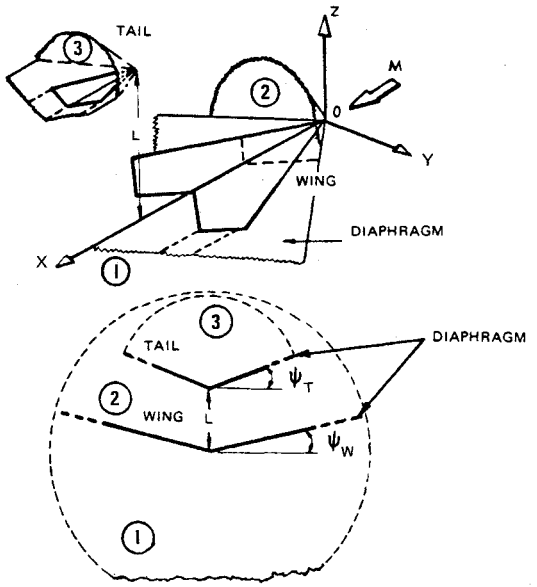


**Fig. 5 Zones in wing-tail configuration.**

where

$$\tau = (\bar{\xi}^2 - \bar{\lambda}^2)^{1/2} \geq 0 \quad \text{and} \quad \theta = \sin^{-1}\bar{\eta}/\tau$$

The significance of $\tau$ and $\theta$ is illustrated in Fig. 4. Substitution of Eqs. (11) and (12) into Eq. (6) yields

$$C_{\bar{\nu}\bar{\mu}\bar{\lambda}} = -\frac{1}{\pi}\int_{\bar{\xi}_L}^{\bar{\xi}_U} \exp(-ik_1\bar{\xi})[F(\tau,\bar{\eta}_U) - F(\tau,\bar{\eta}_L)]\,d\bar{\xi} \quad (13)$$

$C_{\bar{\nu}\bar{\mu}\bar{\lambda}}$ can be evaluated from this expression using numerical integration technique, since $F$ is closely approximated by the first few terms of the infinite summation in Eq. (12).

The limit of integration $\bar{\xi}_U, \bar{\xi}_L, \bar{\eta}_U, \bar{\eta}_L$ are determined by the location of the box with respect to the Mach hyperbola (see Fig. 4). If the box is cut by the Mach hyperbola, only that part of the box upstream of the Mach hyperbola contributes to the value of the AIC.

In general the integration limits may be summarized in the following way:

$$\bar{\eta}_U = \text{Minimum of } \bar{\mu} + 1/2 \text{ or } (\bar{\xi}^2 - \bar{\lambda}^2)^{1/2}$$

$$\bar{\eta}_L = \text{Maximum of } \bar{\mu} - 1/2 \text{ or } (\bar{\xi}^2 - \bar{\lambda}^2)^{1/2}$$

$$\bar{\xi}_U = \bar{\nu} + 1/2$$

$$\bar{\xi}_L = \begin{cases} \text{Maximum of } \bar{\nu} - 1/2 \text{ or } [(\bar{\mu} - 1/2)^2 + \bar{\lambda}^2]^{1/2} \\ \qquad\qquad \text{if } \bar{\mu} > 1/2 \\ \text{Maximum of } \bar{\nu} - 1/2 \text{ or } \bar{\lambda} \text{ if } \bar{\mu} < 1/2 \end{cases} \quad (14)$$

**b) Development of $W_{\bar{\nu}\bar{\mu}\bar{\lambda}}$, $V_{\bar{\nu}\bar{\mu}\bar{\lambda}}$, and $U_{\bar{\nu}\bar{\mu}\bar{\lambda}}$**

As written, Eqs. (8, 9, and 10) imply that $W_{\bar{\nu}\bar{\mu}\bar{\lambda}}$, $V_{\bar{\nu}\bar{\mu}\bar{\lambda}}$, and $U_{\bar{\nu}\bar{\mu}\bar{\lambda}}$ are obtained by differentiating $C_{\bar{\nu}\bar{\mu}\bar{\lambda}}$. $C_{\bar{\nu}\bar{\mu}\bar{\lambda}}$, however, is a numerically evaluated approximation, and is not suitable for differentiation; furthermore, differentiation tends to increase the effects of rounding errors and approximations. Therefore, the expressions for $W_{\bar{\nu}\bar{\mu}\bar{\lambda}}$, $V_{\bar{\nu}\bar{\mu}\bar{\lambda}}$, and $U_{\bar{\nu}\bar{\mu}\bar{\lambda}}$ are manipulated to a form which required only integration.

Substituting Eq. (13) into Eq. (8) and applying the Leibnitz Theorem for differentiation of an integral yields

$$W_{\bar{\nu}\bar{\mu}\bar{\lambda}} = -\frac{1}{\pi}\Big[\int_{\bar{\xi}_L}^{\bar{\xi}_U} \frac{\partial}{\partial\bar{\lambda}}\{\exp(-i\bar{k}_1\bar{\xi})[F(\tau,\bar{\eta}_U) - F(\tau,\bar{\eta}_L)]\}d\bar{\xi} + \{\exp(-i\bar{k}_1\bar{\xi})[F(\tau,\bar{\eta}_U) - F(\tau,\bar{\eta}_L)]\partial\bar{\xi}/\partial\bar{\lambda}\}\Big|_{\bar{\xi}_L}^{\bar{\xi}_U}\Big] \quad (15)$$

Now, $\tau = [\bar{\xi}^2 - \bar{\lambda}^2]^{1/2}$; therefore

$$\partial\tau/\partial\bar{\lambda} = -(\bar{\lambda}/\bar{\xi})\partial\tau/\partial\bar{\xi}$$

In Eq. (15), since $\bar{\eta}_U$ and $\bar{\eta}_L$ are functions of $\tau$, one may obtain

$$\partial F(\tau,\bar{\eta}_U)/\partial\bar{\lambda} = -(\bar{\lambda}/\bar{\xi})\partial F(\tau,\bar{\eta}_U)/\partial\bar{\xi} \text{ etc.} \quad (16)$$

$$W_{\bar{\nu}\bar{\mu}\bar{\lambda}} = \frac{1}{\pi}\Big[\bar{\lambda}\int_{\bar{\xi}_L}^{\bar{\xi}_U} \exp(-i\bar{k}_1\bar{\xi})(1 + i\bar{k}_1\bar{\xi})\{F(\tau,\bar{\eta}_U) - F(\tau,\bar{\eta}_L)\}/\bar{\xi}^2 d\bar{\xi} + \bar{\lambda}\{\exp(-i\bar{k}_1\bar{\xi})[F(\tau,\bar{\eta}_U) - F(\tau,\bar{\eta}_L)]/\bar{\xi}\}\Big|_{\bar{\xi}_L}^{\bar{\xi}_U} + \{\exp(-i\bar{k}_1\bar{\xi})[F(\tau,\bar{\eta}_U) - F(\tau,\bar{\eta}_L)]\partial\bar{\xi}/\partial\bar{\lambda}\}\Big|_{\bar{\xi}_L}^{\bar{\xi}_U}\Big] \quad (17)$$

By applying the limits of integration [Eq. (14)] for this expression, Eq. (17) can be written,

$$W_{\bar{\nu}\bar{\mu}\bar{\lambda}} = \frac{\lambda}{\pi}\Big[\int_{\bar{\xi}_L}^{\bar{\xi}_U} \exp(-ik_1\bar{\xi})(1 + i\bar{k}_1\bar{\xi})/\bar{\xi}^2\{F(\tau,\bar{\eta}_U) - F(\tau,\bar{\eta}_L)\}d\bar{\xi} + \{\exp(-i\bar{k}_1\bar{\xi})[F(\tau,\bar{\eta}_U) - F(\tau,\bar{\eta}_L)]\}\Big|_{\bar{\xi}_L}^{\bar{\xi}_U}\Big] \quad (18)$$

Similarly, Eq. (9) gives

$$V_{\bar{\nu}\bar{\mu}\bar{\lambda}} = -\frac{M}{\pi\bar{k}_1}\Big[\Big(\frac{\exp(-ik_1\bar{\xi})}{\bar{\xi}}\{\partial\bar{\eta}_U/\partial\bar{\mu}\,\sin\frac{\bar{k}_1}{M}(\bar{\xi}^2 - \bar{\eta}^2 - \bar{\lambda}^2)^{1/2} - \partial\bar{\eta}_L/\partial\bar{\mu}\,\sin\frac{\bar{k}_1}{M}(\bar{\xi}^2 - \bar{\eta}^2 - \bar{\lambda}^2)^{1/2}\}\Big|_{\bar{\xi}_L}^{\bar{\xi}_U} + \int_{\bar{\xi}_L}^{\bar{\xi}_U} \partial\bar{\eta}_U/\partial\bar{\mu}\,\sin\frac{\bar{k}_1}{M}(\bar{\xi}^2 - \bar{\eta}^2 - \bar{\lambda}^2)^{1/2} - \partial\bar{\eta}_L/\partial\bar{\mu}\,\sin\frac{\bar{k}_1}{M}(\bar{\xi}^2 - \bar{\eta}^2 - \bar{\lambda}^2)^{1/2}\Big)\frac{(1 + i\bar{k}_1\bar{\xi})}{\bar{\xi}^2}\exp(-i\bar{k}_1\bar{\xi})d\bar{\xi}\Big] \quad (19)$$

It will be seen that evaluation of Eq. (19) will be troublesome when $\bar{k}_1 = 0$. Consequently, Eq. (19) is remanipulated in the limit as $\bar{k}_1 \to 0$, by applying L'Hospital

rule, which yields

$$\lim_{\bar{k}_1 \to 0} V_{\bar{\nu}\bar{\mu}\bar{\lambda}} = -\frac{1}{\pi} \log \left| \frac{\bar{\xi} + (\bar{\xi}^2 - \bar{\eta}_U^2 - \bar{\lambda}^2)^{1/2}}{\bar{\xi} + (\bar{\xi}^2 - \bar{\eta}_L^2 - \bar{\lambda}^2)^{1/2}} \right| \frac{(\partial \bar{\eta}_U / \partial \bar{\mu})}{(\partial \bar{\eta}_L / \partial \bar{\mu})} \Bigg|_{\bar{\xi}_L}^{\bar{\xi}_U} \quad (20)$$

By analogy, Eq. (10) will be

$$U_{\bar{\nu}\bar{\mu}\bar{\lambda}} = -\frac{1}{\pi}[\partial \bar{\xi}_U / \partial \bar{\nu})(F(\tau, \bar{\eta}_U) - F(\tau, \bar{\eta}_L))_{\bar{\xi} = \bar{\xi}_U} \exp(-i\bar{k}_1 \bar{\xi}_U) - \partial \bar{\xi}_L / \partial \bar{\nu}(F(\tau, \bar{\eta}_U) - F(\tau, \bar{\eta}_L))_{\bar{\xi} = \bar{\xi}_L} \exp(-i\bar{k}_1 \bar{\xi}_L)] \quad (21)$$

## Velocity Potential and Perturbation Velocity

### Calculations Zones of Influence in Wing-Wing and Wing-Tail Interaction

The region of disturbed flow may be divided into three zones, as shown in Fig. 5. Zone (1) lies below the wing and its diaphragm, and inside the Mach cone emanating from the apex of the wing. It is disturbed only by the sources placed on the lower surface of the wing and wing-diaphragm. Zone (2) lies between the wing and the tail, and inside the wing Mach cone. It is disturbed by the sources placed upon the upper surface of the wing and wing diaphragm and the lower surface of the tail and tail diaphragm. Zone (3) lies above the tail, and inside the tail Mach cone.

The complete solution of the flowfield, then, would consist of separately finding the velocity potential in these three zones. It may be seen, however, that the tail Mach cone lies at least partially inside the wing Mach cone. This has the important implication that the flow ahead of the tail Mach cone is no longer uniform. Use of the set of diaphragms that isolate the upper from the lower half Mach cones of every planar component indeed does permit the use of the usual methods. The upper part of Fig. 6 shows a wing which is pitched at an angle $\alpha$, and a tail which is parallel to the undisturbed flow. The influence of the wing creates a pressure distribution on the tail because the tail is now placed on nonuniform flow. This

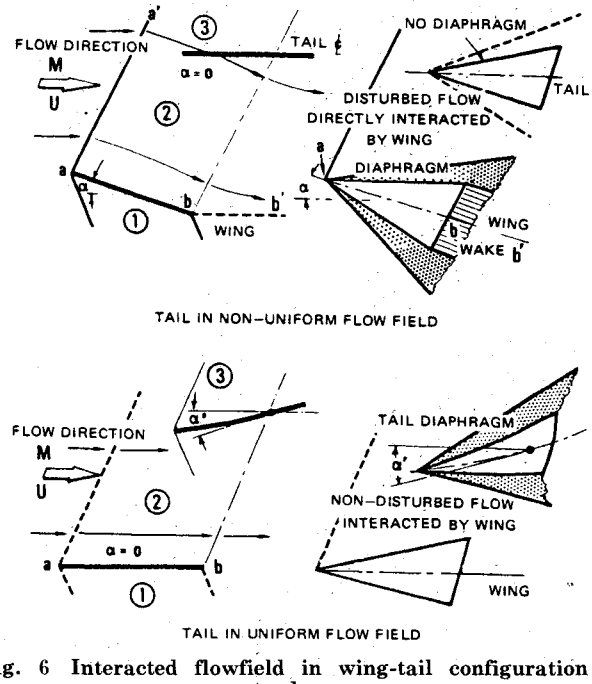


**Fig. 6 Interacted flowfield in wing-tail configuration in steady case.**

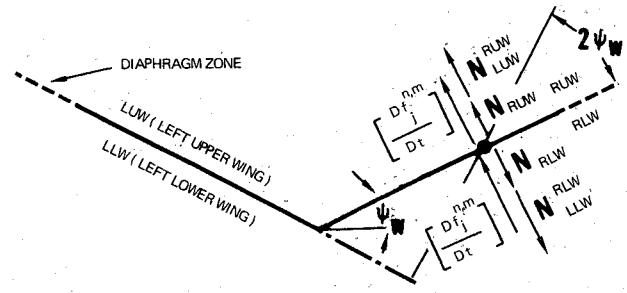


**Fig. 7 Normal wash on surfaces of wing with dihedral.**

pressure distribution can be reproduced on the tail by removing the wing and deforming the tail surface appropriately. The appropriate deformation can then be represented by a source distribution on the tail planform upper and lower surfaces which cancels exactly the flow disturbance caused by the wing, thus satisfying the boundary condition on the tail. This source distribution in turn gives rise to a distribution on the tail diaphragm so that the upper and lower tail surfaces can be considered noncommunicative. It may be observed that there is no further influence on the tail diaphragm from the wing.

## Boundary Value Problem in the Interfered Flowfield

### Single Wing with Dihedral

Consider a single wing with dihedral illustrated in Fig. 7. If $f_j^{n,m}$ is the modal deflection at box $(n,m)$ in mode $j$, then

$$b_1/U\, D f_j^{n,m}/Dt = D\bar{f}_j^{n,m}/Dt = [ik_1 f_j^{n,m} + b_1 \partial f_j^{n,m}/\partial x] \quad (22)$$

where $\bar{f}_j^{n,m} = (b_1/U) f_j^{n,m}$ = scaled modal deflection. The flow tangency condition at $(n,m)$ which lies on the upper surface of the right wing is

$$D\bar{f}_j^{n,m}/Dt = (N_{RUW}^{n,m} + \hat{N}_{\substack{RUW \\ LUW}}^{n,m}) \quad (23)$$

where $\hat{N}_{RUW(LUW)}^{n,m}$ is the complex outward normal wash at $(n,m)$ induced by the source distribution over the upper surface of the left wing, given by

$$\hat{N}_{\substack{RUW \\ LUW}}^{n,m} = \sum_{\substack{\text{left} \\ \text{wing} + \\ \text{diaphragm}}} [W_{\bar{\nu}\bar{\mu}\bar{\lambda}}^{(RW)_{(LW)}} \cos 2\Psi_W - V_{\bar{\nu}\bar{\mu}\bar{\lambda}}^{(RW)_{(LW)}} \sin 2\Psi_W] N_{LUW}^{\nu\mu} \quad (24)$$

The local source strength is then found by Eq. (23) and is

$$N_{RUW}^{n,m} = D\bar{f}^{n,m}/Dt - \hat{N}_{\substack{RUW \\ LUW}}^{n,m} \quad (25)$$

Similarly, for the box $(n,m)$ on the lower surface of the right wing

$$N_{RLW}^{n,m} = -D\bar{f}^{n,m}/Dt - \hat{N}_{\substack{RLW \\ LLW}}^{n,m} \quad (26)$$

where

$$\hat{N}_{\substack{RLW \\ LLW}}^{n,m} = -\sum_{\substack{\text{left} \\ \text{wing} + \\ \text{diaphragm}}} [W_{\bar{\nu}\bar{\mu}\bar{\lambda}}^{(RW)_{(LW)}} \cos 2\psi_W - V_{\bar{\nu}\bar{\mu}\bar{\lambda}}^{(RW)_{(LW)}} \sin 2\psi_W] N_{LLW}^{\nu\mu} \quad (27)$$

The negative signs appearing in Eqs. (26) and (27) are illustrated in Fig. 7. The boundary conditions for the off-

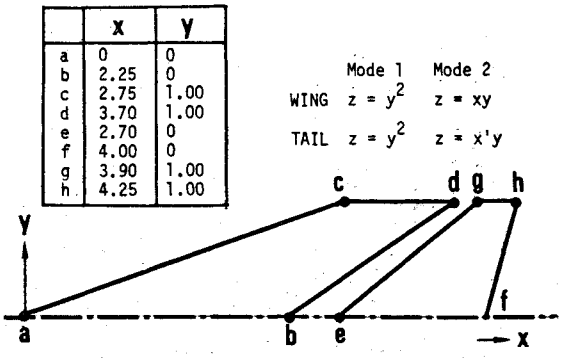


Fig. 8 AGARD wing-tail configuration.

wing and wake diaphragms are expressed by Eqs. (2) and (3).

The nondimensional velocity potential distribution on either wing planform and diaphragm is related to the local normal washes (source strength) through

$$\Delta\bar{\bar{\phi}}_j^{n,m} = \sum_{\substack{\text{right}\\ \text{wing +}\\ \text{diaphragm}}} [C_{\bar{\nu}\bar{\mu}o}(N_{RUW}{}^{\nu\mu} - N_{RLW}{}^{\nu\mu}) + \sum_{\substack{\text{left}\\ \text{wing +}\\ \text{diaphragm}}} C_{\bar{\nu}\bar{\mu}\lambda}\{\pm\}(N_{RUW}{}^{\nu\mu} - N_{RLW}{}^{\nu\mu}) \quad (28)$$

where (+) and (−) signs correspond to symmetric and antisymmetric mode, respectively.

The source strength difference at box $(n,m)$ on the diaphragm can be found by solving Eq. (28). All the source strengths ahead of box $(n,m)$ are known and the velocity potential is given by Eqs. (2) and (3).

$$(N_{RUW}{}^{n,m} - N_{RLW}{}^{n,m}) = C_{ooo}{}^{-1}\Delta\bar{\bar{\phi}}_j^{n,m} - \sum_{\substack{\text{right wing}\\ \text{ahead +}\\ \text{diaphragm}}} C_{\bar{\nu}\bar{\mu}o}(N_{RUW}{}^{\nu\mu} - N_{RLW}{}^{\nu\mu}) + \sum_{\substack{\text{left wing}\\ \text{+ diaphragm}}} C_{\bar{\nu}\bar{\mu}\lambda}{}^{(RW)}_{(LW)}\{\pm\}(N_{RUW}{}^{\nu\mu} - N_{RLW}{}^{\nu\mu}) \quad (29)$$

An additional condition to be satisfied is the continuity of mass flow (or total normal wash) across the diaphragm, that is,

$$N_{RUW}{}^{n,m} + N_{RLW}{}^{n,m} = -\hat{N}_{LUW}{}^{n,m} + \hat{N}_{LLW}{}^{n,m} \quad (30)$$

Equations (29) and (30) can now be solved simultaneously to give the source strength on the upper and lower surfaces of box $(n,m)$.

The source strengths found on the upper and lower surfaces are in general, different in magnitude. (For the case of zero dihedral, they will differ in sign but not in magnitude, in which case only the upper surface need be considered.)

## Wing and Tail with Dihedral and Vertical Separation

After completing the solution for wing with dihedral and wing wake region, the solution for tail with dihedral and vertical and horizontal separations is performed. The source strength difference used to satisfy the boundary condition of tangential flow for boxes on the tail surface is given

$$N_{RUT}{}^{n,m} - N_{RLT}{}^{n,m} = 2\frac{D\bar{f}^{n,m}}{Dt} + \hat{N}_{LLT}{}^{n,m} - \hat{N}_{LUT}{}^{n,m} - 2\hat{N}_{RW}{}^{n,m} - 2\hat{N}_{LW}{}^{n,m} \quad (31)$$

where $\hat{N}_{RUT(LUT)}{}^{n,m}$ and $\hat{N}_{RLT(LLT)}{}^{n,m}$ are computed in a similar manner as in Eqs. (24) and (26), and

$$\hat{N}_{LW}{}^{n,m}_{RUT} = \sum_{\substack{\text{left wing}\\ \text{+ diaphragm}}} [\cos(\psi_T + \psi_W)\, W_{\bar{\nu}\bar{\mu}\lambda}{}^{(RT)}_{(LW)} - \sin(\psi_T + \psi_W) V_{\bar{\nu}\bar{\mu}\lambda}{}^{(RT)}_{(LW)}]N_{LW}{}^{\nu\mu} \quad (32)$$

where

$$N_{LW}{}^{\nu\mu} = \{\pm\}\begin{cases} N_{RUW}{}^{\nu\mu} & \text{if } L > 0 \text{ or } L = 0 \text{ and } \psi_T - \psi_W > 0 \\ N_{RLW}{}^{\nu\mu} & \text{if } L < 0 \text{ or } L = 0 \text{ and } \psi_T - \psi_W < 0 \end{cases} \quad (33)$$

and

$$\hat{N}_{RW}{}^{n,m}_{RUT} = \sum_{\substack{\text{right}\\ \text{wing +}\\ \text{diaphragm}}} [\cos(\psi_T - \psi_W) W_{\bar{\nu}\bar{\mu}\lambda}{}^{(RT)}_{(RW)} - \sin(\psi_T - \psi_W) V_{\bar{\nu}\bar{\mu}\lambda}{}^{(RT)}_{(RW)}]N_{RW}{}^{\nu\mu} \quad (34)$$

where $N_{RW}{}^{\nu\mu}$ is obtained in a manner similar to that in Eq. (33). Then the velocity potential difference is found in the usual manner.

$$\Delta\bar{\bar{\phi}}_j^{n,m} = \sum_{\substack{\text{right}\\ \text{tail +}\\ \text{diaphragm}}} C_{\bar{\nu}\bar{\mu}o}(N_{RUT}{}^{\nu\mu} - N_{RLT}{}^{\nu\mu}) + \sum_{\substack{\text{left}\\ \text{tail +}\\ \text{diaphragm}}} C_{\bar{\nu}\bar{\mu}\lambda}{}^{(RT)}_{(LT)}\{\pm\}(N_{RUT}{}^{\nu\mu} - N_{RLT}{}^{\nu\mu}) \quad (35)$$

For diaphragm boxes, the source strength can be determined by a similar manner to that shown in Eqs. (29) and (30).

## Pressure Distributions, Generalized Forces, and Generalized Aerodynamic Coefficients

### Pressure Distributions

Once the velocity potential difference is evaluated over a surface, the pressure distribution for the $j$th mode is

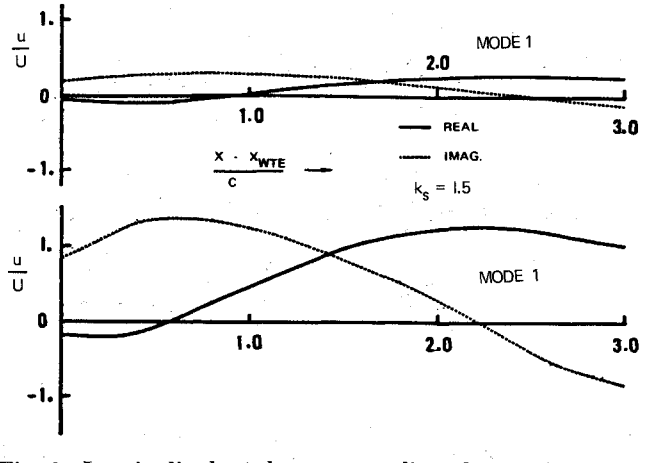


Fig. 9 Longitudinal wash on a sampling chord, $y/s = 0.72$, $z/s = 0.1$.

found by differentiating $\Delta\phi_j$.

$$\Delta\bar{C}_{pj}{}^{n,m} = \frac{\Delta\bar{p}_j}{q} = \frac{2}{\alpha^{n,m}b_1\beta}\left[\Delta\bar{\bar{\phi}}_j(x,y)\Big|_{x_{LE}}^{x_{TE}} + i\alpha^{n,m}k_1\Delta\bar{\bar{\phi}}^{n,m}\right] \quad (36)$$

where the velocity potential difference $\Delta\bar{\bar{\phi}}_j(x,y)$ is evaluated at the leading and trailing edges of box $(n,m)$ by interpolation between the value for box $(n,m)$ and the values for boxes directly ahead or behind. The on-planform area of each box is $\alpha^{n,m}(b_1{}^2/\beta)$.

The lift on each box due to a unit generalized deflection of $j$th mode is given by

$$\bar{L}^{n,m} = q\,\frac{b_1}{\beta}\,\bar{L}_j{}^{n,m} \quad (37)$$

The total lift is obtained through algebraic summation over the wing planforms.

### Generalized Forces

The presence of the differentiation with respect to $x$ in the pressure expression makes it preferable to calculate the generalized forces directly from the velocity potential, rather than by integration of the pressure distributions weighted by the various modal functions. This may be accomplished as follows. If $f_i(x,y)$ is the $i$th modal deflection in nondimensional form, the generalized force associated with each box $(n,m)$, as a result of the pressure for the $j$th mode is

$$\bar{Q}_{ij}{}^{n,m} = \iint_{A(n,m)} f_i(x,y)\Delta\bar{p}_j(x,y)dxdy \quad (38)$$

or, by substituting Eq. (36) into Eq. (38), one obtains

$$\bar{Q}_{ij}{}^{n,m} = 2q\left(\frac{b_1{}^2}{\beta}\right)\frac{\alpha^{n,m}}{b_1\beta}ik_1f_i{}^{n,m}\Delta\bar{\bar{\phi}}_j{}^{n,m} + \frac{1}{\alpha^{n,m}}\left[f_i(x,y)\Delta\bar{\bar{\phi}}_j(x,y)\Big|_{x_{LE}}^{x_{TE}} - b_1\Delta\bar{\bar{\phi}}_j{}^{n,m}\frac{\partial f_i{}^{n,m}}{\partial x}\right] \quad (39)$$

The total generalized force in the $i$th mode due to unit generalized deflection of the $j$th mode is thus an algebraic summation over the boxes on either wing or tail surface.

## Numerical Examples

### Unsteady Aerodynamics Applications

A typical wing-tail configuration has been specified by the AGARD of NATO and is shown in Fig. 8, for use in comparison of various aerodynamic theories and experimental results. For the case of a wing alone, the values of longitudinal wash, sidewash, and upwash plotted along the sample chord located at a spanwise distance of 0.72 $s$ and vertical distance of 0.1 $s$ are given in Figs. 9, 10, and 11. These values, computed at the reduced frequency $k_s$ = 1.5 and $M$ = 1.56, are due to antisymmetric torsion mode. The smoothing technique is applied, also. The pressure distributions for the wing-tail configuration, in which the tail dihedral is 30°, $M$ = 1.56, and $k_s$ = 1.5 with a combined longitudinal and vertical separation, are given in Fig. 12. In these computations, the nonoscillating tail is placed parallel to the uniform flow and is exposed to the interacted flow caused by the wing pitch mode.

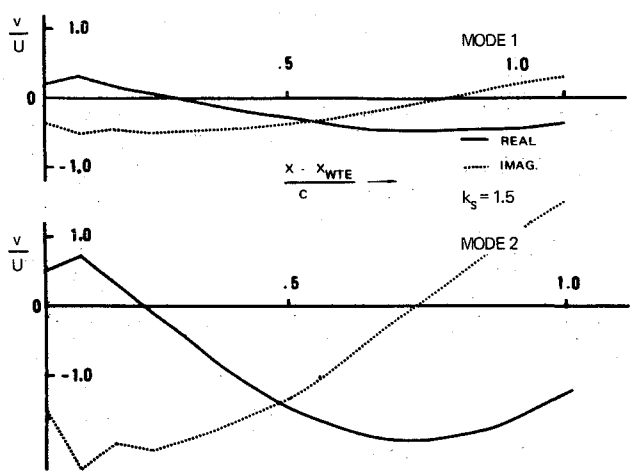


Fig. 10 Sidewash on a sampling chord.

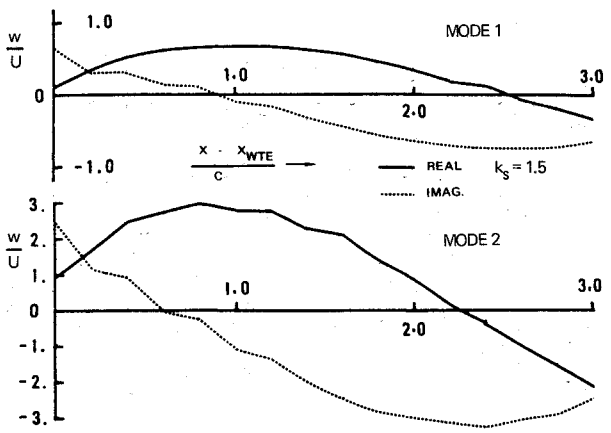


Fig. 11 Upwash on a sampling chord.

### Flutter Model Application

Flutter model test data used in this correlation study are obtained from the tests conducted in the Cornell Aeronautical Laboratory 8 ft × 8 ft variable density transonic wind tunnel.[2] The supersonic tests are conducted having both models contained in the same plane with a very small longitudinal clearance gap between the models. Table 1 tabulates the computed flutter speeds and test data for the 45° and 60° swept models under various flow conditions. The flutter modes were found to be composed of wing bending coupled with fuselage torsion for all of the analysis cases with the exception of configuration 23 at $M$ = 1.232 where the flutter mode contained a high frequency torsion mode. Figure 13 shows computed flutter speed and frequency vs horizontal separation. This effect is much smaller than the effect of vertical separation on flutter speed and frequency shown in Fig. 14. In this case, the tail is moved out of the strongest influence of oscillating wing wake; therefore reducing wing interference loads on the tail is beneficial on the flutter speed.

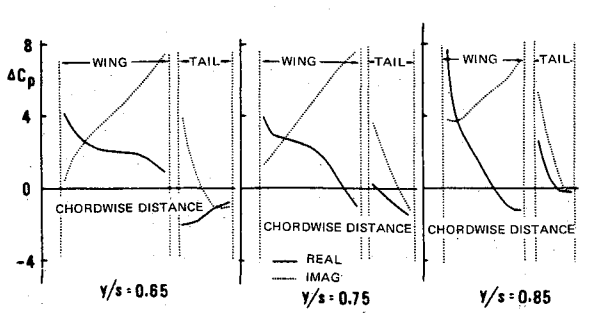


Fig. 12 Chordwise pressure distributions, moderate separations, due to wing pitch mode, $M$ = 1.56, $k_s$ = 1.5.

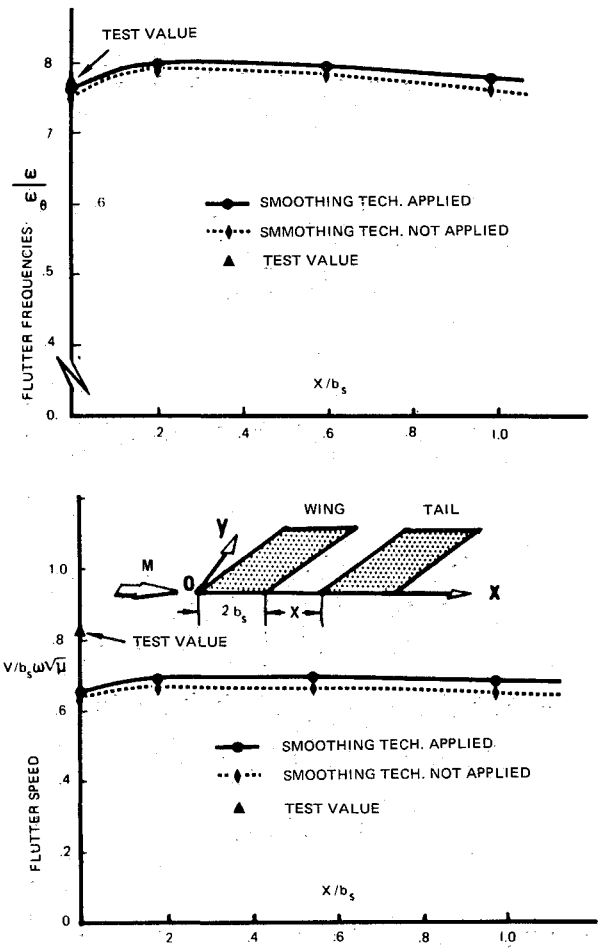


Fig. 13 Flutter speed and frequency vs horizontal separations for 45° sweep model (Conf. 15), $x/b_s = 0.505$, $M = 1.238$.

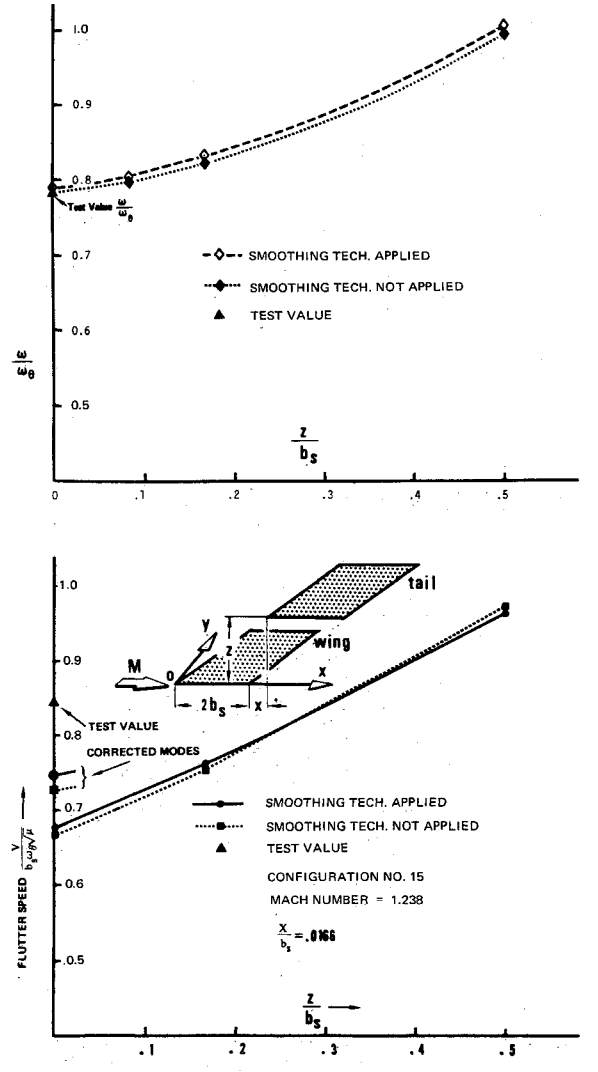


Fig. 14 Flutter speed and frequency vs vertical separations for 45° sweep model (Conf. 15), $x/b_s = 0.505$, $M = 1.238$.

## Conclusions

Theoretical studies for evaluating the unsteady loadings on nonplanar wing-tail configurations of elastic aircraft in supersonic flow have been made. the computational scheme developed for the unsteady loadings appears to provide reasonable results when applied to analysis configurations that meet the restrictions of the Mach box method. Through these studies, the spatial AIC's associ-

Table 1 Analytical and test flutter results on configurations 15, 22, and 23

| | | | | | | | | Theoretical results | | | | | Test results | | | |
|---|---|---|---|---|---|---|---|---|---|---|---|---|---|---|---|---|
| ANA No. | CON No. | $M$ | $\frac{\omega_\theta}{\omega_h}$ | $X/b_s$ | $Z/b_s$ | $\mu$ | $\rho$ Slug/ft$^3$ ($\times 10^4$) | Modes modified | $V_f$ fps | $\eta_f$ cps | $\frac{V_f}{b_s\omega_\theta\sqrt{\mu}}$ | $\frac{\omega}{\omega_\theta}$ | $V_f$ fps | $\eta_f$ cps | $\frac{V_f}{b_s\omega_\theta\sqrt{\mu}}$ | $\frac{\omega}{\omega_\theta}$ |
| | 15 | 1.238 | 1.765 | .021 | 0.0 | 50.9 | 3.5 | | | | | | 1254.0 | 26.0 | .8460 | .788 |
| 3 | | | | .167 | 0.0 | | | No | [a]1006.8 | 26.5 | .6799 | .8035 | | | | |
| | | | | | | | | | 1001.1 | 26.27 | .6760 | .7959 | | | | |
| 21 | | | | .167 | 0.0 | | | Yes | 1103.6 | 27.60 | .7454 | .8363 | | | | |
| | | | | | | | | | 1094.3 | 27.26 | .7389 | .8260 | | | | |
| | 22 | 1.240 | 1.428 | .0257 | 0.0 | 65.3 | 2.7 | | | | | | 1317.0 | 20.8 | .7880 | .842 |
| 13 | | | | .190 | 0.0 | | | No | 1139.8 | 23.70 | .6817 | .9594 | | | | |
| | | | | | | | | | 1058.7 | 22.46 | .6332 | .9091 | | | | |
| 22 | | | | .190 | 0.0 | | | Yes | 1205.4 | 24.25 | .7210 | .9821 | | | | |
| | | | | .190 | 0.0 | | | | 1138.01 | 23.28 | .6806 | .9427 | | | | |
| | 23 | 1.232 | 1.775 | .0257 | 0.0 | 36.7 | 4.8 | | | | | | 1292.0 | 24.2 | .8290 | .788 |
| 18 | | | | .190 | 0.0 | | | No | 1063.2 | 30.95 | .6821 | 1.008 | | | | |
| | | | | | | | | | 1094.8 | 31.03 | .7024 | 1.011 | | | | |
| 23 | | | | .190 | 0.0 | | | Yes | 1083.5 | 31.17 | .6951 | 1.015 | | | | |
| | | | | | | | | | 1123.5 | 30.98 | .7209 | 1.009 | | | | |

[a]The first line of the theoretical results for each case denotes the results in which the smoothing technique (refinement) is applied.

ated with velocity potential, upwash, sidewash, and longitudinal wash at the center of the arbitrarily oriented pulse-receiving panel are developed, since these values become singular at the Mach hyperbola, some manipulation applying the Bessel function series to render it amenable to numerical integration has been done. The basic process of solving an interfered flow problem is shown by considering the various noncommunicative zones and their bounding surfaces, and the various physical conditions to be satisfied by source distributions on these surfaces. The boundary conditions to be satisfied in these interfered flowfields are the flow tangency condition on the lifting surface and continuity concepts of mass and pressure on the diaphragm region, respectively. Since there are no analytical methods available for obtaining "exact" unsteady supersonic airloads on any three-dimensional, wing-tail configuration in the interfered flowfield, only a qualitative evaluation can be made. The effects of longitudinal separation on flutter speed and frequency ratio indicate that only a small variation in flutter velocity is obtained for relatively large values of longitudinal separation. There is a fairly large increase in flutter speed and frequency ratio with vertical separation. Presently, no test data are available for these separations in supersonic flow; however, the subsonic test results support these trends.[2,15] The study also reveals that the inclusion of airfoil thickness effects results in a very small reduction in flutter speed. Although the theoretical-experimental trends are similar, it appears that the theory is conservative and may be due to unknown effects such as shocks attached on the wing and tail leading-trailing edges, or may be due to flow blockage over the tail due to the wings presence in these critical low Mach numbers.

The method developed for evaluating the unsteady loadings on nonplanar wings and wing-tail configurations in supersonic flow appears to provide reasonable results and can contribute significantly both to the knowledge and handling quality of advanced supersonic aircraft and to the application of the space shuttle.

## References

[1]Topp, L. J., Rowe, W. S., and Shattuck, A. W., "Aeroelastic Considerations in the Design of Variable Sweep Airplanes," *Proceedings of the ICAS/RAES,* International Council of the Aeronautical Sciences, 1966, London, England.

[2]Balcerak, J. C., "Flutter Tests of Variable Sweep Configurations," AFFDL-TR-68-101, Sept. 1968, AFFDL, Wright-Patterson Air Force Base, Ohio.

[3]Sensburg, O. and Lashka, B., "Flutter Induced by Aerodynamic Interference between Wing and Tail," *Journal of Aircraft,* Vol. 7, No. 4, July–Aug. 1970, pp. 319–324.

[4]Mykytow, W. J., Noll, T. E., Huttsell, L. J., and Shirk, M. H., "Investigations Concerning the Coupled Wing-Fuselage-Tail Flutter Phenomenon," *Journal of Aircraft,* Vol. 9, No. 1, Jan. 1972, pp. 48–54.

[5]Pines, S., Dujundji, J., and Neuringer, J., "Aerodynamic Flutter Derivatives for a Flexible Wing with Supersonic and Subsonic Edges," *Journal of the Aeronautical Sciences,* Vol. 22, No. 10, Oct. 1955, pp. 693–700.

[6]Zartarian, G. and Hsu, P. T., "Theoretical Studies on the Prediction of Unsteady Supersonic Airloads on Elastic Wings," WADC TR 56-97, Feb. 1956, Wright Air Development Center, Wright-Patterson Air Force Base, Ohio.

[7]Ii, J. M., "A Refined Prediction Method for the Unsteady Aerodynamics of Supersonic Elastic Aircraft," *Journal of Aircraft,* Vol. 9, No. 1, Jan. 1972, pp. 61–68.

[8]Andrew, L. V. and Moore, M. T., "Further Developments in Supersonic Aerodynamic Influence Coefficient Methods," *Proceedings of the AIAA Symposium on Structural Dynamics and Aeroelasticity,* AIAA, New York, 1966.

[9]Ashley, H. and Zartarian, G., "Piston Theory—A New Tool for the Aeroelastician," *Journal of the Aeronautical Sciences,* Vol. 23, No. 12, Dec. 1956, pp. 1109–1118.

[10]Ii, J. M., Borland, C. J., and Hogley, J. R., "Prediction of Unsteady Aerodynamic Loadings of Non-Planar Wings and Wing-Tail Configurations in Supersonic Flow," AFFDL TR-71-108, March 1972, AFFDL, Wright-Patterson Air Force Base, Ohio.

[11]Garrick, I. E. and Rubinow, S. I., "Theoretical Study of Air Forces on an Oscillating or Steady Thin Wing in a Supersonic Main Stream," Rept. 872, June 1947, NACA.

[12]Evvard, J. C., "Use of Source Distributions for Evaluating Theoretical Aerodynamics of Thin Finite Wings at Supersonic Speeds," Rept. 951, 1950, NACA.

[13]Andrew, L. V. and Moore, M. T., "Unsteady Aerodynamics for Advanced Configurations," TDR 64-152, May 1965, AFFDL, Wright-Patterson Air Force Base, Ohio.

[14]Ashley, H., "Supersonic Airloads on Interfering Lifting Surfaces by Aerodynamic Influence Coefficient Theory," Boeing Document D2-22067TN, 1962, Boeing Co., Seattle, Wash.

[15]Albano, E., Perkinson, F., and Rodden, W. P., "Subsonic Lifting-Surface Theory Aerodynamics and Flutter Analysis of Interfering Wing/Horizontal-Tail Configurations," AFFDL-TR-70-59, Sept. 1970, AFFDL, Wright-Patterson Air Force Base, Ohio.